

Article

# CO<sub>2</sub> Hydrogenation to Methanol over La<sub>2</sub>O<sub>3</sub>-Promoted CuO/ZnO/Al<sub>2</sub>O<sub>3</sub> Catalysts: A Kinetic and Mechanistic Study

Marios Kourtelesis , Kalliopi Kousi  and Dimitris I. Kondarides \*

Department of Chemical Engineering, University of Patras, 26504 Patras, Greece; mkourtelesis@chemeng.upatras.gr (M.K.); kousikalliopi@yahoo.com (K.K.)

\* Correspondence: dimi@chemeng.upatras.gr; Tel.: +30-261-0969-527

Received: 21 December 2019; Accepted: 31 January 2020; Published: 3 February 2020

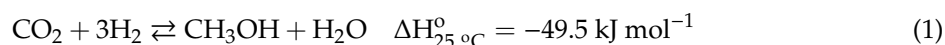


**Abstract:** The hydrogenation of CO<sub>2</sub> to methanol has been investigated over CuO/ZnO/Al<sub>2</sub>O<sub>3</sub> (CZA) catalysts, where a part of the Al<sub>2</sub>O<sub>3</sub> (0, 25, 50, 75, or 100%) was substituted by La<sub>2</sub>O<sub>3</sub>. Results of catalytic performance tests obtained at atmospheric pressure showed that the addition of La<sub>2</sub>O<sub>3</sub> generally resulted in a decrease of CO<sub>2</sub> conversion and in an increase of methanol selectivity. Optimal results were obtained for the CZA-La50 catalyst, which exhibited a 30% higher yield of methanol, compared to the un-promoted sample. This was attributed to the relatively high specific surface area and porosity of this material, the creation of basic sites of moderate strength, which enhance adsorption of CO<sub>2</sub> and intermediates that favor hydrogenation steps, and the ability of the catalyst to maintain a large part of the copper in its metallic form under reaction conditions. The reaction mechanism was studied with the use of in situ infrared spectroscopy (DRIFTS). It was found that the reaction proceeded with the intermediate formation of surface formate and methoxy species and that both methanol and CO were mainly produced via a common formate intermediate species. The kinetic behavior of the best performing CZA-La50 catalyst was investigated in the temperature range 190–230 °C as a function of the partial pressures of H<sub>2</sub> (0.3–0.9 atm) and CO<sub>2</sub> (0.05–0.20 atm), and a kinetic model was developed, which described the measured reaction rates satisfactorily.

**Keywords:** CO<sub>2</sub> hydrogenation; CuO/ZnO/Al<sub>2</sub>O<sub>3</sub> catalyst; La<sub>2</sub>O<sub>3</sub> promoter; DRIFTS; reaction mechanism; kinetic model

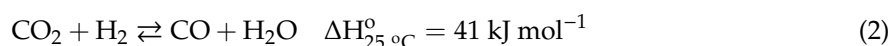
## 1. Introduction

Carbon dioxide, which is one of the main greenhouse gases and a major contributor to global warming, has been identified as a promising feedstock for producing valuable chemicals [1], and its efficient utilization is expected to contribute toward the development of a carbon-neutral energy cycle [2]. One of the most investigated processes aiming at this direction is hydrogenation of CO<sub>2</sub> to methanol (Equation (1)) using H<sub>2</sub> coming from renewable energy sources.



Methanol is one of the most important chemicals as it can be used directly as a fuel, as an energy carrier in fuel cells, or as a raw material for the synthesis of products such as formaldehyde, acetic acid, and olefins [3]. Methanol is traditionally produced from syngas. However, for obvious economic and environmental reasons, there is great interest in developing a process where methanol is produced from abundant and inexpensive CO<sub>2</sub>. The main problem that is currently hindering the wider application of the latter process is the low methanol selectivity due to the occurrence of the competitive reverse

water-gas shift (RWGS) reaction (Equation (2)) [4]. Thus, it is important to develop catalytic materials characterized by high activity and selectivity toward methanol.



The state-of-the-art catalyst for the title reaction is CuO/ZnO/Al<sub>2</sub>O<sub>3</sub> (CZA), where CuO and ZnO catalyze both the methanol synthesis and the WGS reaction [5]. A plethora of studies have been reported dealing with the reaction kinetics and mechanism over CZA-based materials, and several models have been proposed to explain the experimental results [6–9]. However, there is still debate regarding the reaction mechanism and catalyst requirements [4,10,11]. As far as catalysts are concerned, efforts have been made to improve the performance of CZA by either replacing/doping Cu with noble metals (e.g., Pt, Pd) [12–15] or by adding oxides in order to enhance the adsorption properties of the support and to increase the dispersion of the Cu phases [16–21]. This is the reason why the majority of studies pinpoint some sort of coupling in the mechanism between the copper phase and the support oxide, with the latter being the anchor point for one of the oxygen atoms of CO<sub>2</sub> [22,23]. In this respect, several promoters have been studied, mainly oxides of metals such as Mn, La, Zr, Cr, and B [21,24–28]. In several cases, the catalytic performance of CZA catalysts was enhanced following substitution of part or all of Al<sub>2</sub>O<sub>3</sub> by oxides, such as ZrO<sub>2</sub>, Cr<sub>2</sub>O<sub>3</sub>, Ga<sub>2</sub>O<sub>3</sub>, or SiO<sub>2</sub> [29–31]. Results were explained considering that, for example, ZrO<sub>2</sub> improves the dispersion of copper particles, SiO<sub>2</sub> enhances the long-term stability of the catalyst, whereas dopants such as Cr<sub>2</sub>O<sub>3</sub> or Ga<sub>2</sub>O<sub>3</sub> increase the specific activity per unit Cu surface area [29–31].

In the present work, a series of La-promoted CZA catalysts (CZA-La<sub>x</sub>) of variable La<sub>2</sub>O<sub>3</sub>-to-Al<sub>2</sub>O<sub>3</sub> ratios was synthesized, characterized, and tested for the title reaction. Results showed that the addition of La<sub>2</sub>O<sub>3</sub> increased the selectivity toward methanol and that the yield of methanol was maximized for the CZA-La50 catalyst, for which 50% of Al<sub>2</sub>O<sub>3</sub> was replaced by La<sub>2</sub>O<sub>3</sub>. This was explained considering that the addition of La<sub>2</sub>O<sub>3</sub> affected the distribution and strength of basic sites on the catalyst surface and promoted the formation of metallic copper under the reaction conditions. Results of in situ DRIFTS experiments indicated that the reaction proceeds via the intermediate formation of surface formate and methoxy species. The kinetic behavior of the best performing catalyst was investigated as a function of the reaction temperature and partial pressures of H<sub>2</sub> and CO<sub>2</sub>, and a kinetic model was developed, which described the measured reaction rates satisfactorily.

## 2. Results

### 2.1. Characteristics of the Synthesized Catalysts

CuO/ZnO/Al<sub>2</sub>O<sub>3</sub> and La-promoted CZA catalysts were synthesized by a co-precipitation method, as described in Section 4.1. The molar composition of the unpromoted CZA catalyst was 61.7% CuO, 30.1% ZnO, and 8.2% Al<sub>2</sub>O<sub>3</sub>. The La-promoted samples were prepared by substituting different portions of Al<sub>2</sub>O<sub>3</sub> by La<sub>2</sub>O<sub>3</sub>. The catalysts thus prepared are denoted in the following as CZA-La<sub>x</sub>, where *x* (0, 25, 50, 75, or 100) indicates the molar fraction (%) of Al<sub>2</sub>O<sub>3</sub> replaced by La<sub>2</sub>O<sub>3</sub> (Table 1).

**Table 1.** Textural properties of the synthesized CuO/ZnO/Al<sub>2</sub>O<sub>3</sub> (CZA)-La<sub>x</sub> catalysts.

Catalyst	Specific Surface Area (m <sup>2</sup> g <sup>-1</sup> )	Pore Volume (cm <sup>3</sup> g <sup>-1</sup> )	Pore Size (nm)
CZA-La0	111	0.70	20
CZA-La25	88	0.78	30
CZA-La50	96	0.79	30
CZA-La75	61	0.45	27
CZA-La100	47	0.32	25

The textural properties of the as-synthesized CZA-Lax catalysts are summarized in Table 1. It was observed that, as a general trend, the increase of the  $\text{La}_2\text{O}_3$  content resulted in a decrease of the specific surface area (SSA), which dropped from  $111 \text{ m}^2 \text{ g}^{-1}$  for the un-promoted sample to  $47 \text{ m}^2 \text{ g}^{-1}$  for the CZA-La100 catalyst, for which  $\text{Al}_2\text{O}_3$  was fully substituted by  $\text{La}_2\text{O}_3$ . This confirmed the higher ability of  $\text{Al}_2\text{O}_3$  to act as a structural stabilizing agent of the  $\text{CuO}/\text{ZnO}$  catalyst, compared to  $\text{La}_2\text{O}_3$ . It is of interest to note, however, that the CZA-La50 sample retained a relatively large SSA and exhibited the highest pore volume and pore size among the catalysts investigated (Table 1).

In Figure 1A are shown the X-ray diffraction (XRD) patterns of the freshly prepared catalysts. It was observed that all materials were characterized by peaks attributable to  $\text{CuO}$  and  $\text{ZnO}$  phases, with the most intense ones located at  $2\theta = 35.5^\circ$ ,  $38.6^\circ$ ,  $31.8^\circ$ , and  $34.3^\circ$ , respectively. The absence of clearly resolved peaks corresponding to  $\text{Al}_2\text{O}_3$  and  $\text{La}_2\text{O}_3$  phases may be explained considering the low content of these oxides and indicated that they exist in an amorphous or microcrystalline state [32]. Qualitatively similar results have been reported for La-modified  $\text{CuO-ZnO-Al}_2\text{O}_3/\text{HZSM-5}$  catalysts synthesized by the co-precipitation method [21].

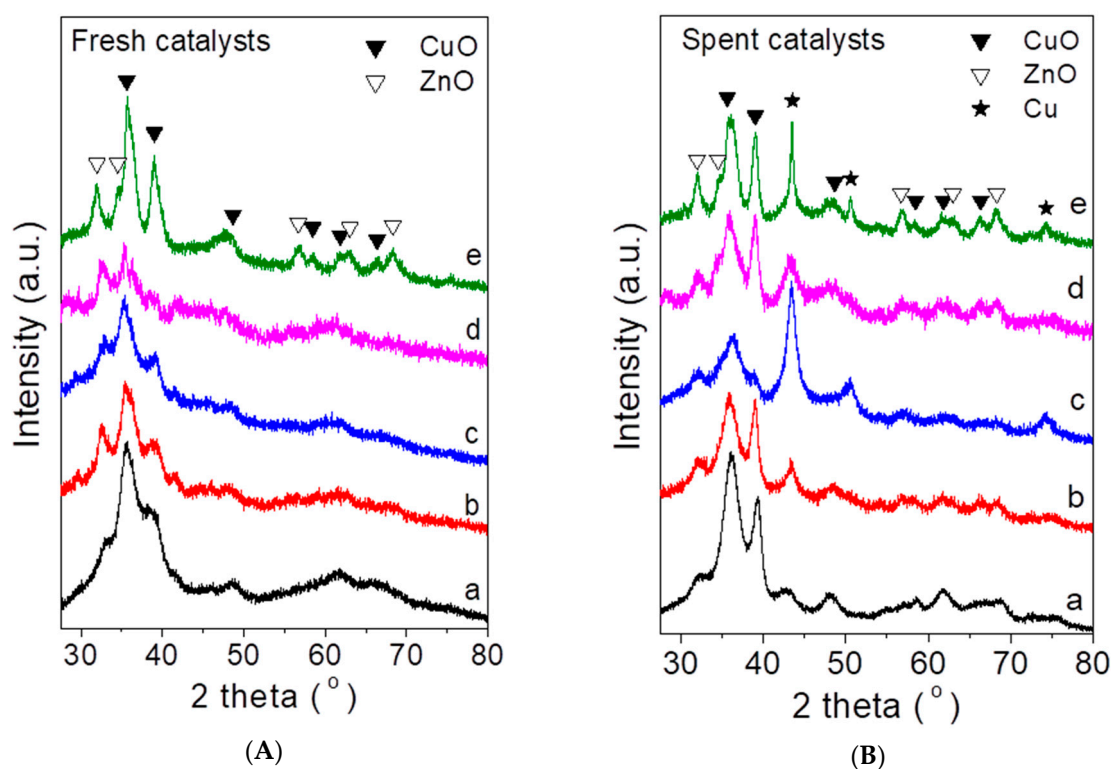


**Figure 1.** XRD patterns obtained for (A) the freshly prepared and (B) the spent CZA-Lax catalysts: (a)  $x = 0$ ; (b)  $x = 25$ ; (c)  $x = 50$ ; (d)  $x = 75$ ; (e)  $x = 100$ .

The XRD patterns obtained following the exposure of the catalyst samples to the reaction conditions are shown in Figure 1B. It was observed that, in all cases, the diffractograms were characterized by the presence of additional peaks located at  $2\theta = 43.5^\circ$  and  $50.5^\circ$ , attributable to metallic copper ( $\text{Cu}^0$ ), which is known to be an active component for methanol synthesis [33,34]. It is of interest to note that the relative intensity of the  $\text{Cu}^0$  peaks, compared to those of  $\text{CuO}$ , was generally higher for the La-promoted catalysts and was maximized for the CZA-La50 sample (c), which, as discussed below, exhibited the highest yield toward methanol.

The surface basicity of the pre-reduced catalysts was studied by temperature-programmed desorption of  $\text{CO}_2$  ( $\text{CO}_2$ -TPD), and the results obtained are shown in Figure 2. It was observed that the desorption profile of the unpromoted CZA-La0 catalyst (a) was characterized by an intense low-temperature (LT) peak centered at ca.  $85^\circ\text{C}$  and a broad high-temperature (HT) shoulder extending

up to 300 °C. The LT peak could be assigned to weak basic sites related to surface hydroxyl groups, whereas the HT shoulder could be attributed to basic sites of moderate strength corresponding to metal-oxygen pairs (Al–O, Zn–O, and/or Cu–O) [35,36].

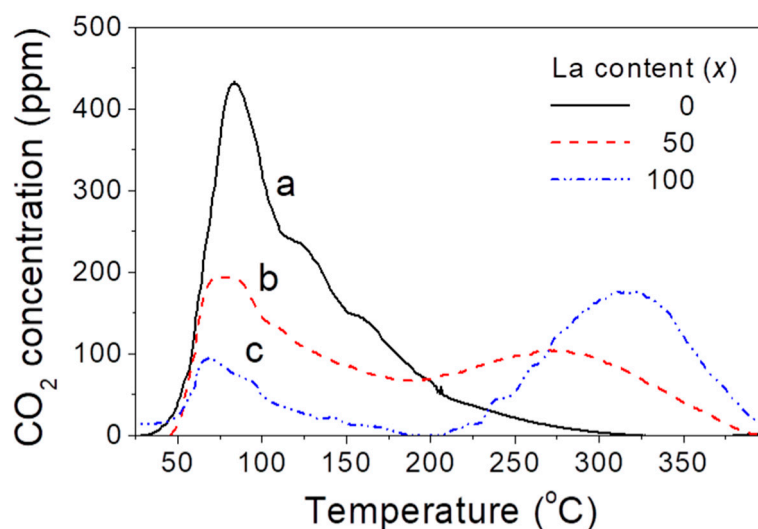


**Figure 2.** CO<sub>2</sub>-temperature-programmed desorption (TPD) profiles obtained for the pre-reduced CZA-Lax catalysts: (a)  $x = 0$ ; (b)  $x = 50$ ; (c)  $x = 100$ .

Substitution of 50% or 100% of Al<sub>2</sub>O<sub>3</sub> by La<sub>2</sub>O<sub>3</sub> (b and c, respectively) resulted in a substantial decrease of the intensity of the LT peak, indicating that weak basic sites were mainly related to the OH groups of alumina. This was accompanied by a progressive growth and shift of the HT shoulder toward higher temperatures. The total amount of desorbed CO<sub>2</sub>, calculated by integration of the corresponding TPD curves, decreased from 25.9 μmol/g for CZA-La0 to 23.1 μmol/g for CZA-La50 and to 18.1 μmol/g for the CZA-La100 catalyst. This indicated that the total number of basic sites decreased following the addition of La<sub>2</sub>O<sub>3</sub>. On the other hand, it is evident from Figure 2 that both the relative concentration and strength of the HT basic sites increased with increasing La content. This showed that the La-promoted catalysts were characterized by a higher amount of basic sites of moderate strength, the number and strength of which increased with increasing La<sub>2</sub>O<sub>3</sub> content. Qualitatively similar results have been reported for Cu/ZnO catalysts promoted with Fe or Ga [36].

## 2.2. Catalytic Performance Tests

The catalytic performance of the CZA-Lax samples was investigated at atmospheric pressure in the temperature range of 160–260 °C. Under these reaction conditions, the only carbon-containing products detected were methanol and CO, and no catalyst deactivation was observed with time-on-stream. The yield of methanol was typically lower than 1% because, according to the Le Chatelier principle, Reaction (1) is favored at high pressures. Typical results obtained over the best performing CZA-La50 catalyst are shown in Figure 3 and are compared with those of the CZA-La0 and CZA-La100 samples. It was observed that, in all cases, conversion of CO<sub>2</sub> ( $X_{CO_2}$ ) increased with the increase of the reaction temperature (Figure 3A). Substitution of Al<sub>2</sub>O<sub>3</sub> by La<sub>2</sub>O<sub>3</sub> resulted in a decrease of  $X_{CO_2}$ , which took its lowest values for the CZA-La100 catalyst. Selectivity toward methanol ( $S_{CH_3OH}$ ) followed the opposite trend, i.e., it was higher than 90% at 160 °C for all samples and decreased with the increase of temperature, dropping close to zero at ca. 260 °C (Figure 3B) where CO<sub>2</sub> was selectively converted to CO. Interestingly,  $S_{CH_3OH}$  was found to be higher for all La-containing catalysts, compared to un-promoted CZA, and was maximized for the CZA-La100 sample, where Al<sub>2</sub>O<sub>3</sub> was fully substituted by La<sub>2</sub>O<sub>3</sub>. The beneficial effect of La<sub>2</sub>O<sub>3</sub> on methanol selectivity could be attributed to the increase of the concentration of surface basic sites of moderate strength (Figure 2), which are believed to be responsible for catalyzing the C–O bond activation of adsorbed CO<sub>2</sub> species [26–28]. La<sub>2</sub>O<sub>3</sub> also

stabilized copper in its metallic form under reaction conditions (Figure 1), which is known to promote the title reaction. A similar beneficial effect on methanol selectivity was reported for La-promoted Cu/ZnO/ZrO<sub>2</sub> catalysts [37], as well as for Cu/ZnO catalysts promoted with other basic oxides, such as CeO<sub>2</sub> [38].

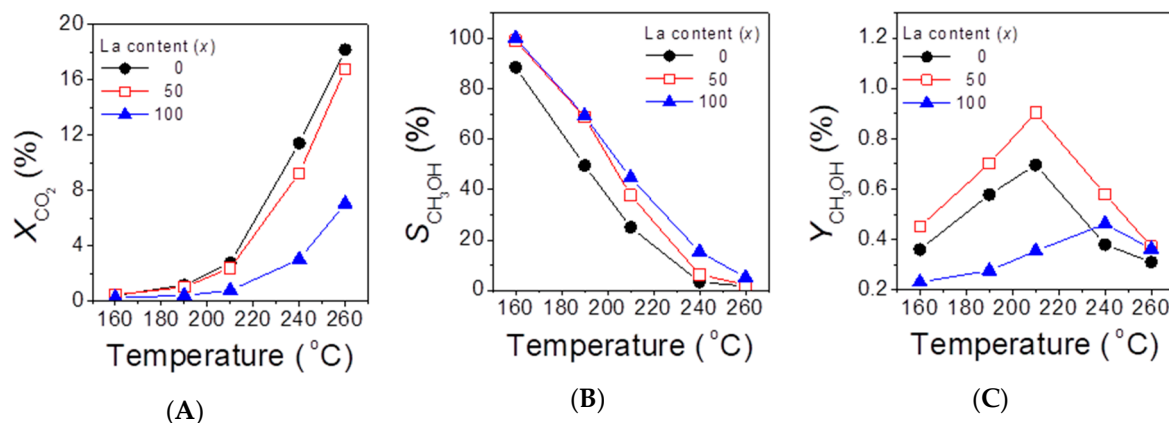


**Figure 3.** (A) Conversion of CO<sub>2</sub>, (B) selectivity to methanol, and (C) yield of methanol as functions of the reaction temperature obtained over CZA-La<sub>x</sub> catalysts with  $x = 0, 50$ , or  $100$ . Experimental conditions: mass of catalyst: 200 mg; total flow rate: 50 cm<sup>3</sup> min<sup>-1</sup>; feed composition: 10% CO<sub>2</sub> and 90% H<sub>2</sub>.

As a result of the counteracting effects of temperature on CO<sub>2</sub> conversion and methanol selectivity, the yield of methanol went through a maximum at temperatures around 210 °C (Figure 3C). As mentioned above, optimal results were obtained for the CZA-La50 catalyst, which combined high activity and selectivity, leading to a yield of methanol of 0.9% at 210 °C, which was ca. 30% higher than that of the un-promoted CZA-La0 sample (0.7%).

### 2.3. In Situ DRIFTS Studies

The in situ diffuse reflectance infrared Fourier-transform (DRIFT) spectra obtained following the interaction of carbon monoxide with CZA-La0 and CZA-La50 catalysts are presented in Figure 4. Adsorption and desorption of CO was investigated not only because CO is a reaction product, but also because it is a suitable probe molecule to study the nature and strength of active sites. As shown in Figure 4A, exposure of the pre-reduced CZA-La0 catalyst to CO at 25 °C for 30 min (a) resulted in the appearance of bands located at ca. 2170 and 2108 cm<sup>-1</sup>, which were attributed to gas-phase CO [39,40]. The latter peak also contained a contribution from carbonyl species linearly adsorbed on metallic Cu, which are known to vibrate in this region [41]. Switching the feed to He resulted in the removal of the bands due to gas-phase CO and in the appearance of the Cu-CO peak at 2105 cm<sup>-1</sup>, which slightly decreased in intensity with time-on-stream (b–d). The increase of temperature under He flow at 100 °C resulted in a substantial decrease of the peak intensity (e). A further increase of temperature resulted in the disappearance of the peak (f,g), indicating that carbonyl species were weakly adsorbed on the catalyst surface.

Similar DRIFT spectra obtained over the CZA-La50 catalyst are presented in Figure 4B. It was observed that the carbonyl peak (b) appeared at a higher wavenumber (2110 cm<sup>-1</sup>) and was of lower intensity, compared to CZA-La0 (Figure 4A), indicating that it was less strongly adsorbed on Cu. This was verified by the disappearance of the peak upon increasing the temperature to 100 °C (e). Comparison of the spectra obtained over the un-promoted (Figure 4A) and the La-containing sample (Figure 4B) indicated that the presence of La<sub>2</sub>O<sub>3</sub> resulted in a decrease of the adsorption strength of Cu toward CO.

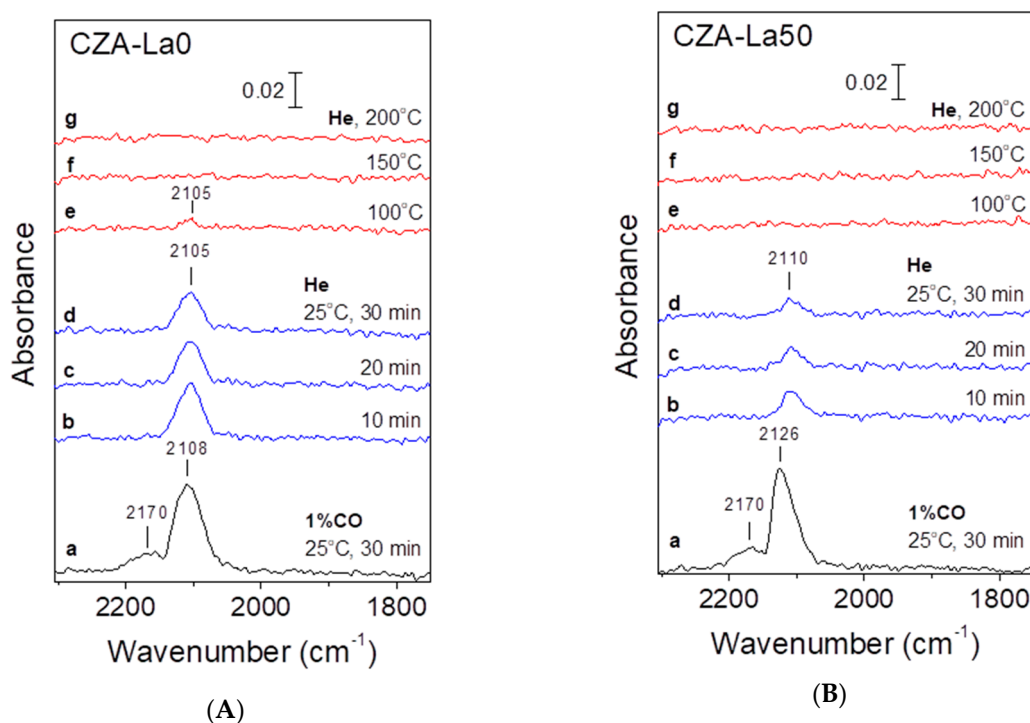


**Figure 4.** DRIFT spectra obtained over (A) the CZA-La0 and (B) the CZA-La50 catalyst following interaction with 1% CO (in He) at room temperature (a), purging with He for 30 min (b–d), and subsequent stepwise heating under He flow at temperatures up to 200 °C (e–g).

The formation and fate of surface species formed under reaction conditions was investigated over the CZA-La0 and the CZA-La50 catalysts by in situ DRIFT spectroscopy in the temperature range 25–400 °C, and the results obtained are presented in Figure 5A,B. In the same figure is also shown the evolution of products in the gas-phase, which was monitored in separate experiments performed under the same reaction conditions with the use of the transient-MS technique (Figure 5C,D).

Regarding the CZA-La0 catalyst (Figure 5A), it was observed that exposure of the pre-reduced sample to the CO<sub>2</sub>/H<sub>2</sub> mixture at 25 °C (a) resulted in the appearance of a peak located at 2108 cm<sup>-1</sup>, attributed to CO adsorbed on metallic Cu (see above), a band centered at ca. 1640 cm<sup>-1</sup> attributed to adsorbed water [39,42], and a broad feature centered at ca. 3450 cm<sup>-1</sup>, which was due to adsorbed OH species [41]. The appearance of these bands indicated that the gas-phase CO<sub>2</sub> adsorbed dissociatively on the catalyst surface at room temperature to yield adsorbed CO and adsorbed oxygen species. The latter combined with dissociatively adsorbed hydrogen to form hydroxyl species and then H<sub>2</sub>O [39]. Two additional bands located at 1588 and 1390 cm<sup>-1</sup> could be assigned to adsorbed formate (HCOO) species [42].

The stepwise increase of temperature at 200 °C (b–d) resulted in the disappearance of all spectral features mentioned above. The fact that gas-phase products started evolving at this temperature (Figure 5C) indicated that these surface species were active intermediates for the title reaction. It should be noted that, in addition to CO, small amounts of methanol were also produced in the gas-phase at temperatures around 200 °C, but due to the low concentration of reactants and the transient nature of the experiments presented in Figure 5C, the methanol concentration was close to the detection limit of the apparatus and could not be quantified. A further increase of temperature at 400 °C (e–h) resulted in the development of two bands at 2125 and 2175 cm<sup>-1</sup> due to the gas-phase CO, the production of which was favored at high temperatures because of the endothermic nature of the RWGS reaction. At temperatures higher than ca. 450 °C, measurable amounts of CH<sub>4</sub> also appeared in the gas-phase (Figure 5C). It should be noted that the DRIFT spectra obtained at temperatures higher than 200 °C (Figure 5A,d–h) were characterized by a change of the background signal in the range 1250–1600 cm<sup>-1</sup>,

which resulted in the appearance of a “negative” curve in this region. This was most possibly due to the (partial) oxidation of Cu by product  $H_2O$ , which is a strong oxidant at elevated temperatures. A qualitatively similar behavior was observed for the CZA-La50 sample (Figure 5B).

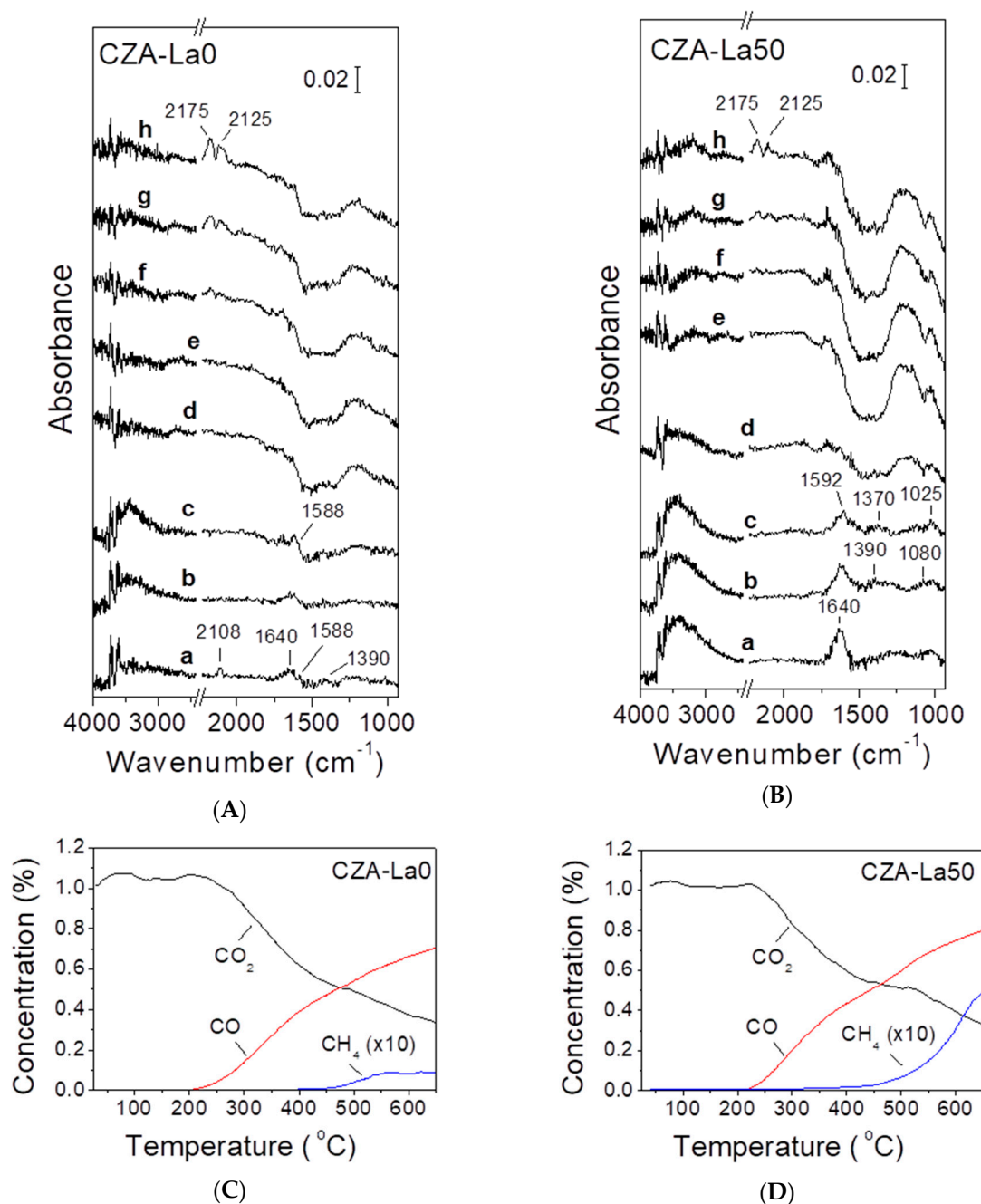


**Figure 5.** In situ DRIFT spectra obtained over (A) the CZA-La0 and (B) the CZA-La50 catalyst following interaction with a reaction mixture consisting of 1%  $CO_2$  and 9%  $H_2$  (in He) at (a) 25 °C and stepwise heating at: (b) 100 °C; (c) 150 °C; (d) 200 °C; (e) 250 °C; (f) 300 °C; (g) 350 °C; (h) 400 °C. The transient-MS spectra obtained over the CZA-La0 and CZA-La50 catalyst under the same conditions are shown in (C) and (D), respectively.

The in situ DRIFT spectra obtained over the CZA-La50 catalyst under reaction conditions are shown in Figure 5B. Similar to the un-promoted sample, exposure to the  $CO_2/H_2$  mixture at 25 °C (a) resulted in the development of bands attributed to adsorbed water (1640  $cm^{-1}$ ) and OH species (broad band at 3450  $cm^{-1}$ ). However, the carbonyl band at ca. 2110  $cm^{-1}$  did not appear over this

catalyst, probably because of the weak adsorption of this species on the CZA-L50 catalyst, compared to CZA-La0 (see Figure 4). The increase of the reaction temperature to 100 °C (b) and 150 °C (c) resulted in the development of bands at 1592, 1390, and 1370  $\text{cm}^{-1}$  due to adsorbed formate ( $\text{HCOO}$ ) species, as well as in the appearance of bands at ca. 1025 and 1080  $\text{cm}^{-1}$ , attributable to surface methoxy ( $\text{CH}_3\text{O}$ ) species [41,42]. The intensity of these bands decreased upon further increasing temperature to 200 °C (d), i.e., in the temperature range where methanol was produced (Figure 3) and diminished at higher temperatures (e–h). This indicated that  $\text{CO}_2$  hydrogenation to methanol occurred with the intermediate formation of formate and methoxy species, in agreement with the results of previous studies [42]. For the reasons mentioned above, the amount of methanol produced in the gas-phase at temperatures around 200 °C was very low and, therefore, was not shown in the transient-MS results presented in Figure 5D. On the other hand,  $\text{CO}$  evolved in the gas-phase at temperatures higher than 200 °C and was accompanied by the formation of relatively small amounts of  $\text{CH}_4$  at temperatures above ca. 350 °C (Figure 5D).

#### 2.4. Reaction Kinetics

The initial rates of methanol and  $\text{CO}$  evolution were measured at atmospheric pressure over the best performing CZA-La50 catalyst in the temperature range of 190–230 °C. The results obtained with the use of different feed compositions are summarized in Figure 6, where symbols correspond to the measured values and solid curves represent their fitting according to the kinetic model discussed below (see Section 3.2). It was observed that the increase of the partial pressure of  $\text{H}_2$  ( $P_{\text{H}_2}$ ) in the range 0.3–0.9 atm at a constant partial pressure of  $\text{CO}_2$  ( $P_{\text{CO}_2} = 0.1$  atm) did not affect appreciably the rate of  $\text{CO}$  evolution at a given temperature (Figure 6A), but resulted in an almost linear increase of the methanol formation rate (Figure 6B). On the other hand, the increase of  $P_{\text{CO}_2}$  in the range 0.05–0.20 atm at constant  $P_{\text{H}_2} = 0.8$  atm resulted in a progressive increase of both the rate of  $\text{CO}$  (Figure 6C) and methanol (Figure 6D) production.

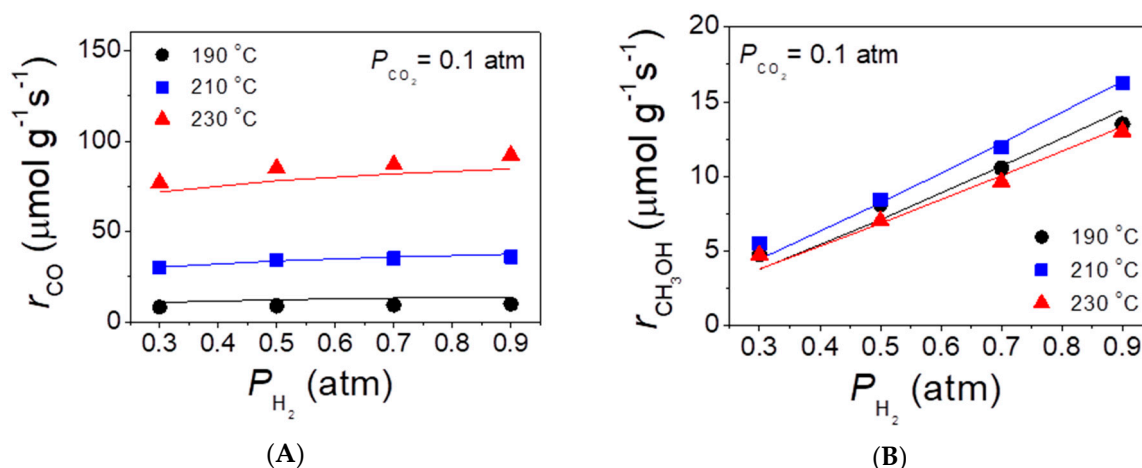
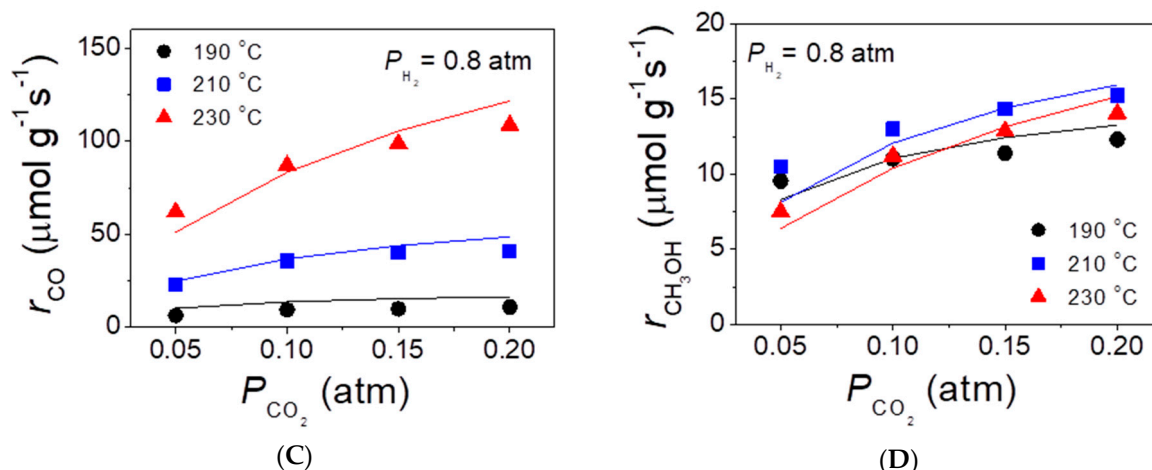


Figure 6. Cont.



**Figure 6.** Effects of the partial pressure of H<sub>2</sub> in the feed at the constant partial pressure of CO<sub>2</sub> (A,B) and of the partial pressure of CO<sub>2</sub> at constant partial pressure of H<sub>2</sub> (C,D) on the rates of CO (A,C) and methanol (B,D) evolution at temperatures of 190, 210, and 230 °C. Solid lines correspond to fitting of experimental results (symbols) with the use of the kinetic model described in Section 3.2.

### 3. Discussion

#### 3.1. Effects of La<sub>2</sub>O<sub>3</sub> Addition on the Characteristics and Performance of Catalysts

The results of the catalyst characterization experiments listed in Table 1 showed that, although replacement of Al<sub>2</sub>O<sub>3</sub> by La<sub>2</sub>O<sub>3</sub> generally resulted in a decrease of the specific surface area, the CZA-La50 sample was characterized by a relatively large SSA and exhibited comparatively high pore volume and pore size. These parameters are known to affect positively the catalytic activity because the increase of SSA results in higher dispersion of the active copper phase, whereas enhanced porosity improves the diffusion of reactants/products to/from the active sites. As a result, conversion of CO<sub>2</sub> over the CZA-La50 catalyst was comparable to that of the un-promoted CZA-La0 sample (Figure 3A).

Regarding selectivity toward methanol, it was substantially improved over the La<sub>2</sub>O<sub>3</sub>-promoted catalysts in the whole temperature range investigated (Figure 3B). This could be related to the ability of La<sub>2</sub>O<sub>3</sub> to enhance the surface basicity of the catalyst [26] and was in agreement with previous results obtained with the use of other basic oxides as dopants [43,44], which showed that basic sites enhanced the adsorption of CO<sub>2</sub> and intermediates and favored hydrogenation of surface formate to methoxy species [26]. As a general trend, a linear relationship was found to exist between the yield of methanol and the CO<sub>2</sub> adsorption capacity of the catalyst [45]. The results of the present CO<sub>2</sub>-TPD experiments (Figure 2) and catalytic performance tests (Figure 3B) indicated that selectivity to methanol increased monotonically with increasing the surface concentration of basic sites of moderate strength. Overall, although Al<sub>2</sub>O<sub>3</sub> elevated CO<sub>2</sub> conversion, it did not benefit the methanol selectivity, probably because it interacted strongly with H<sub>2</sub>O molecules produced during the methanol synthesis reaction, thereby promoting the RWGS reaction to produce CO [38]. On the other hand, the addition of La<sub>2</sub>O<sub>3</sub> improved the selectivity toward methanol, and as a result, the yield of methanol was enhanced over the LCZA-La50 catalyst (Figure 3C).

It is of interest to note that exposure of the CZA-La50 sample to the reaction conditions resulted in the transformation of a larger part of CuO to metallic Cu, compared to the un-promoted CZA-La0 sample (Figure 1B). A similar promotion of the in situ reduction of oxidized copper species (CuO<sub>x</sub>) to Cu<sup>0</sup> was reported for Zr-doped CZA catalysts [46]. This could be explained considering that under reaction conditions, Cu<sup>0</sup> is oxidized to CuO<sub>x</sub> by water, and Cu<sup>0</sup> sites are regenerated by CO and H<sub>2</sub> [47]. When the regeneration rate of Cu<sup>0</sup> sites is not high enough, most of the surface copper sites will be oxidized, thereby resulting in decreased activity [46]. The relatively high content of Cu<sup>0</sup> observed over the “spent” La-promoted samples (Figure 1B) indicated that La<sub>2</sub>O<sub>3</sub> favored the latter reactions

and maintained a larger portion of copper in its metallic form. It may then be suggested that the improved methanol selectivities obtained over the La-promoted catalysts could be related, at least in part, to their ability to keep the content of Cu<sup>0</sup> at high levels under reaction conditions. In this respect, it was proposed that both Cu<sup>+</sup> and Cu<sup>0</sup> were involved in the methanol formation reaction and that catalytic activity depended on the Cu<sup>+</sup>/Cu<sup>0</sup> ratio [8,47–50]. The results of the theoretical calculations indicated that CO<sub>2</sub> hydrogenation to methanol was favored over metallic Cu<sup>0</sup> sites, whereas Cu<sup>+</sup> sites were mainly responsible for the hydrogenation of CO [49]. Further investigation of this issue is beyond the scope of the present work and may be the subject of our future investigation.

### 3.2. Mechanistic Implications and Development of the Kinetic Model

The results presented in Figure 5 showed that exposure of the CZA-La50 catalyst to the CO<sub>2</sub>/H<sub>2</sub> reaction mixture resulted in the formation of surface oxygenated species, in particular formate and methoxy species. Methoxy species, which can be formed by stepwise hydrogenation of formates, are considered as intermediates for the formation of methanol [39,42]. On the other hand, carbon monoxide can be also produced from formate species [39] through decomposition or via the reverse water-gas shift reaction [41]. In the present work, it was suggested that both methanol and CO were produced predominantly via a common formate intermediate, in agreement with the results of previous experimental [51] and theoretical [52] studies.

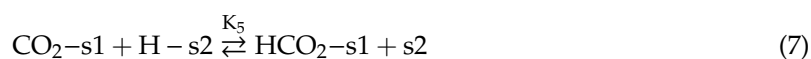
The results of kinetic measurements obtained over the best performing CZA-La50 catalyst (Figure 6) were modeled using a dual-site Langmuir–Hinshelwood mechanism similar to that proposed by Graaf et al. [53,54], taking into account two reactions representing the CO<sub>2</sub> hydrogenation to methanol (Equation (1)) and the water-gas shift reaction (Equation (2)). According to this mechanistic model, CO and CO<sub>2</sub> adsorb competitively on one site (s1), whereas H<sub>2</sub> and H<sub>2</sub>O adsorb competitively on another site (s2). The participation of two different active sites in the CO<sub>2</sub> hydrogenation reaction over Cu/ZnO-based catalysts has been well demonstrated in the literature. It is generally believed that the role of copper is to adsorb hydrogen and deliver atomic hydrogen by spillover, whereas the “support” serves not only as an agent that controls the catalyst texture, but also to adsorb and activate CO<sub>2</sub> [21,26,38,48,50,55,56]. The latter assumption was supported by the present experimental results, which indicated that the addition of La<sub>2</sub>O<sub>3</sub> improved methanol selectivity by increasing the fraction of basic sites of moderate strength on the catalyst surface. This was in agreement with literature results showing that methanol yield was closely related to the number and strength of moderate/strong basic sites, which could be tuned by modification of the support with suitable metal oxides [26,36,57].

According to the above model [53,54], hydrogen adsorbs dissociatively, whereas adsorption of methanol is considered to be negligible. The elementary reaction steps corresponding to this model are described below.

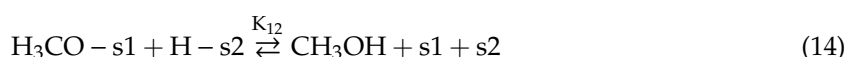
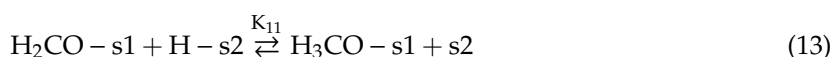
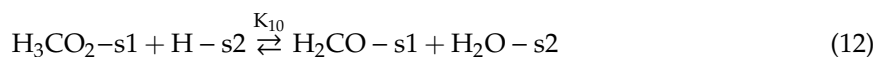
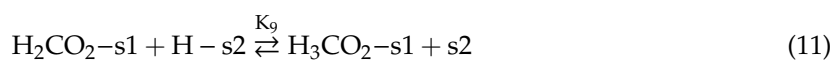
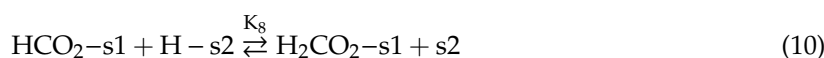
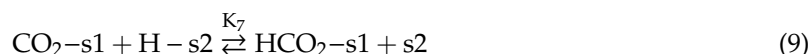
(i) Equilibrium adsorption of reactants and products:



(ii) Water-gas shift reaction (Equation (2)):



(iii) CO<sub>2</sub> hydrogenation to methanol (Equation (1)):



Assuming that the total number of sites s1 and s2 was constant, kinetic expressions were derived by choosing different combinations of surface reactions as rate-determining steps (RDS). The best results were obtained assuming that the RDS were Reaction (7) for the WGS and Reaction (11) for the CO<sub>2</sub> conversion to methanol and that all other reactions were at equilibrium. Accordingly, the reaction rate of the WGS reaction is given by the following expression:

$$r_5 = \frac{k_5 K_1 \sqrt{K_2} \left( P_{\text{CO}_2} \sqrt{P_{\text{H}_2}} - \frac{P_{\text{CO}} P_{\text{H}_2\text{O}}}{K_A \sqrt{P_{\text{H}_2}}} \right)}{\left( 1 + K_1 P_{\text{CO}_2} + K_4 P_{\text{CO}} \right) \left( 1 + \sqrt{K_2 P_{\text{H}_2}} + K_3 P_{\text{H}_2\text{O}} \right)} \quad (15)$$

where  $k_5$  is the kinetic constant of the WGS reaction,  $P_i$  is the partial pressure of compound  $i$  (CO<sub>2</sub>, H<sub>2</sub>, CO, H<sub>2</sub>O), and  $K_A$  is the equilibrium constant of the WGS reaction. Regarding the reaction rate of CO<sub>2</sub> conversion to methanol, it is given by:

$$r_9 = \frac{k_9 K_1 \sqrt{(K_2)^3 K_7 K_8} \left( P_{\text{CO}_2} \sqrt{(P_{\text{H}_2})^3} - \frac{P_{\text{CH}_3\text{OH}} P_{\text{H}_2\text{O}}}{K_B \sqrt{(P_{\text{H}_2})^3}} \right)}{\left( 1 + K_1 P_{\text{CO}_2} + K_4 P_{\text{CO}} \right) \left( 1 + \sqrt{K_2 P_{\text{H}_2}} + K_3 P_{\text{H}_2\text{O}} \right)} \quad (16)$$

where  $k_9$  is the kinetic constant of the reaction,  $P_i$  is the partial pressure of compound  $i$  (CO<sub>2</sub>, H<sub>2</sub>, CO, H<sub>2</sub>O, CH<sub>3</sub>OH), and  $K_B$  is the equilibrium constant of the CO<sub>2</sub> conversion to methanol reaction. Equilibrium constants  $K_A$  and  $K_B$  can be determined from data available in the literature (e.g., [58]).

Since kinetic measurements were obtained in the absence of products in the feed, the initial partial pressures of CH<sub>3</sub>OH, CO, and H<sub>2</sub>O were zero, and, assuming that the terms in the denominator of Equations (15) and (16) were much higher than unity, the above two equations can be simplified as follows to give the initial reaction rates of CO and methanol production:

$$r_{\text{CO}} = r_5 = \frac{k_5 K_1 \sqrt{K_2} P_{\text{CO}_2} \sqrt{P_{\text{H}_2}}}{K_1 P_{\text{CO}_2} + \sqrt{K_2 P_{\text{H}_2}} + K_1 P_{\text{CO}_2} \sqrt{K_2 P_{\text{H}_2}}} \quad (17)$$

$$r_{\text{CH}_3\text{OH}} = r_9 = \frac{k_9 K_1 \sqrt{(K_2)^3 K_7 K_8} P_{\text{CO}_2} \sqrt{(P_{\text{H}_2})^3}}{K_1 P_{\text{CO}_2} + \sqrt{K_2 P_{\text{H}_2}} + K_1 P_{\text{CO}_2} \sqrt{K_2 P_{\text{H}_2}}} \quad (18)$$

The kinetic constants,  $k_i$ , and the equilibrium constants,  $K_i$ , depend on temperature as follows:

$$k_i = A_i \exp\left(-\frac{E_i}{RT}\right) \quad (19)$$

$$K_i = B_i \exp\left(-\frac{\Delta H_i}{RT}\right) \quad (20)$$

where  $A_i$  and  $E_i$  correspond to the pre-exponential factor and the activation energy, respectively, of reaction step  $i$  and  $B_i$  and  $\Delta H_i$  are the pre-exponential factor and the adsorption enthalpy, respectively, of the adsorption of species  $i$ .

The introduction of Equations (19) and (20) to the rate Equations (17) and (18) allows the expression of the reaction rates of CO and methanol production as functions of temperature. The activation energies, pre-exponential factors, and adsorption enthalpies of the reactants were estimated by fitting the experimentally measured reaction rates (Figure 6) using MATLAB, and the values obtained are presented in Table 2. The values of the model parameters satisfied the thermodynamic constraints [59] and were in good agreement with the literature results. For example, the activation energies calculated for CO formation (126.6 kJ/mol) and methanol formation (66.3 kJ/mol) were close to those reported for Cu/ZnO-based catalysts [60].

**Table 2.** Values of the parameters estimated by fitting the reaction rates with Equations (17) and (18).

$k_5$	$k_9$	$K_1$	$K_2$	$K = K_7 \cdot K_8$
$10^{10} \exp\left(-\frac{126,600}{RT}\right)$	$6300 \exp\left(-\frac{66,260}{RT}\right)$	$10^{-7} \exp\left(-\frac{70,000}{RT}\right)$	$10^{-4} \exp\left(-\frac{33,000}{RT}\right)$	$\exp\left(-\frac{0.025}{8.617 \times 10^{-5} T}\right)$

The fitting of the experimental results made according to the rate equations developed for CO and methanol production (Equations (17) and (18)) is shown in Figure 6 (solid lines). It was observed that the proposed kinetic model described the measured reaction rates well. It is the intention of the authors to further test the catalytic performance of the CZA-La50 catalyst at high pressures, relevant to practical applications, and to test the model under these conditions. This will be the subject of our future investigation.

## 4. Materials and Methods

### 4.1. Catalyst Preparation

The CZA-Lax catalysts were synthesized by the co-precipitation method, using  $\text{Cu}(\text{NO}_3)_2 \cdot 3\text{H}_2\text{O}$ ,  $\text{Zn}(\text{NO}_3)_2 \cdot 6\text{H}_2\text{O}$ ,  $\text{Al}(\text{NO}_3)_3 \cdot 9\text{H}_2\text{O}$ , and  $\text{La}(\text{NO}_3)_3 \cdot 6\text{H}_2\text{O}$  (Alfa Aesar, Thermo Fisher (Kandel) GmbH, Kandel, Germany) as metal precursor salts. Weighed amounts of the precursors, calculated to yield the desired metal oxide composition, were dissolved in distilled water, and the solution was heated at 65 °C. This was followed by dropwise addition of the precipitating agent ( $\text{Na}_2\text{CO}_3$  1M) at  $\text{pH } 6.2 \pm 0.1$  under continuous stirring. After aging for 1 h, the precipitate was filtered, washed with distilled water, dried overnight at 80 °C, and finally calcined in air at 300 °C for 3 h.

### 4.2. Catalyst Characterization

The textural properties of the catalysts (specific surface area and porosity) were studied employing nitrogen adsorption at the temperature of liquid  $\text{N}_2$  using a Micromeritics TriStar 3000 instrument. Specific surface areas were calculated using the BET equation for nitrogen relative pressures in the range  $0.06 < P/P_0 < 0.20$ . The pore size distribution was estimated with the Barret–Joyner–Halenda (BJH) method.

X-ray diffraction (XRD) patterns were obtained on a Bruker D8 Advance diffractometer (Billerica, MA, USA) equipped with a Ni-filtered Cu radiation and a LynxEye detector. The diffractograms were recorded in the range  $20^\circ < 2\theta < 80^\circ$  with a scan speed of 0.3 s/step.

### 4.3. In Situ DRIFTS Experiments

The in situ diffuse reflectance infrared Fourier-transform (DRIFT) experiments were performed on a Nicolet 6700 FTIR spectrometer (Waltham, MA, USA) equipped with a DRIFT cell (Spectra Tech),

an MCT detector, and a KBr beam splitter. Typically, the catalyst sample was heated under He flow ( $30 \text{ cm}^3 \text{ min}^{-1}$ ) at  $450 \text{ }^\circ\text{C}$  for 10 min and then reduced with 20%  $\text{H}_2$  in He ( $30 \text{ cm}^3 \text{ min}^{-1}$ ) at  $300 \text{ }^\circ\text{C}$  for 1 h. The adsorbed species were desorbed by heating at  $450 \text{ }^\circ\text{C}$  for 10 min, and the sample was cooled to room temperature. During the cooling stage, background spectra were recorded under He flow at the desired temperatures. The flow was finally switched to the reaction mixture (1%  $\text{CO}_2$  + 9%  $\text{H}_2$  in He,  $30 \text{ cm}^3 \text{ min}^{-1}$ ), and the first spectrum was recorded at  $25 \text{ }^\circ\text{C}$  after 15 min on-stream. The temperature was then step-wise increased up to  $400 \text{ }^\circ\text{C}$ , and spectra were obtained at the desired temperatures after equilibration for 15 min on-stream.

#### 4.4. Transient-MS and $\text{CO}_2$ -TPD Experiments

Temperature-programmed surface reaction experiments coupled with mass spectrometry (transient-MS) were carried out employing the equipment and following the procedures described elsewhere [40]. Briefly, 100 mg of the catalyst sample were placed in a quartz reactor, heated under He flow at  $450 \text{ }^\circ\text{C}$  for 15 min, and then reduced with  $\text{H}_2$  at  $300 \text{ }^\circ\text{C}$  for 1 h. The sample was purged with He at the same temperature for 15 min and finally cooled to room temperature under He flow. Transient experiments were then carried out by switching the flow to the feed composition (1%  $\text{CO}_2$  + 9%  $\text{H}_2$  in He). In all experiments, the total flow rate through the reactor was  $30 \text{ cm}^3 \text{ min}^{-1}$ . The effluent gas composition was monitored on-line with an Omnistar/Pfeiffer Vacuum mass spectrometer (Asstar, Germany).

The temperature-programmed desorption of  $\text{CO}_2$  ( $\text{CO}_2$ -TPD) was studied over catalyst samples previously reduced with hydrogen at  $300 \text{ }^\circ\text{C}$  following the procedure described above. Adsorption of  $\text{CO}_2$  was carried out at room temperature following exposure of the sample to a 1%  $\text{CO}_2$ /He mixture for 1 h. The gas stream was then switched to He ( $30 \text{ cm}^3 \text{ min}^{-1}$ ), and the temperature was increased to  $400 \text{ }^\circ\text{C}$  with a heating rate of  $10 \text{ }^\circ\text{C}/\text{min}$ .

#### 4.5. Catalytic Performance Tests and Kinetic Measurements

The catalytic performance of the synthesized catalysts for the title reaction was evaluated at atmospheric pressure. The fixed-bed reactor employed consisted of a quartz tube (6 mm O.D.) with an expanded 1 cm long section in the middle (8 mm I.D.), containing the catalyst sample. The reaction temperature was measured in the middle of the catalyst bed by means of a K-type thermocouple running through the reactor. The feed composition was controlled with the use of mass-flow controllers. A gas chromatograph (Shimadzu, Kyoto, Japan) equipped with two packed columns (Carboxen, Carbovax) and two detectors (TCD, FID), operating with He as the carrier gas, was used for the analysis of the reactor effluent.

In a typical experiment, 200 mg of a fresh catalyst sample ( $0.18 \text{ mm} < d < 0.25 \text{ mm}$ ) were placed in the reactor and reduced in situ at  $300 \text{ }^\circ\text{C}$  for 1 h under a hydrogen flow of  $50 \text{ cm}^3 \text{ min}^{-1}$ . The temperature was then lowered at  $260 \text{ }^\circ\text{C}$ , and the flow was switched to the reaction mixture (10%  $\text{CO}_2$  + 90%  $\text{H}_2$ , total flow rate:  $50 \text{ cm}^3 \text{ min}^{-1}$ ). The catalyst was conditioned at  $260 \text{ }^\circ\text{C}$  for 30 min, and then, the concentrations of reactants and products were determined by gas chromatography. Similar measurements were carried out following a step-wise lowering of temperature down to  $160 \text{ }^\circ\text{C}$ . Carbon dioxide conversion ( $X_{\text{CO}_2}$ ) and selectivities ( $S_i$ ) toward product  $i$  ( $\text{CH}_4$ ,  $\text{CO}$ ,  $\text{CH}_3\text{OH}$ ) were calculated using the following expressions:

$$X_{\text{CO}_2}(\%) = \frac{C_{\text{CO}_2}^{\text{in}} - C_{\text{CO}_2}^{\text{out}}}{C_{\text{CO}_2}^{\text{in}}} \times 100 \quad (21)$$

$$S_i(\%) = \frac{C_i^{\text{out}}}{C_{\text{CO}_2}^{\text{in}} - C_{\text{CO}_2}^{\text{out}}} \times 100 \quad (22)$$

where  $C_{\text{CO}_2}^{\text{in}}$  and  $C_{\text{CO}_2}^{\text{out}}$  are the concentrations of  $\text{CO}_2$  at the inlet and the outlet of the reactor, respectively.

Intrinsic reaction rates were measured in separate experiments where the conversion of carbon dioxide was kept below 15% so that differential reaction conditions could be assumed, with negligible heat and mass transfer effects. Kinetic experiments were conducted by varying the partial pressure of one reactant, while keeping the partial pressure of the other reactant constant using He as the balance gas. The procedure followed prior to kinetic measurements was similar to that described above for catalytic performance test.

## 5. Conclusions

A set of five La-doped CuO/ZnO/Al<sub>2</sub>O<sub>3</sub> catalysts with variable La<sub>2</sub>O<sub>3</sub> content was synthesized by the co-precipitation method and evaluated for CO<sub>2</sub> hydrogenation toward methanol under atmospheric pressure. The results of catalyst characterization showed that substitution of Al<sub>2</sub>O<sub>3</sub> by La<sub>2</sub>O<sub>3</sub> resulted in a decrease of the specific surface area, which was more evident for samples with high La<sub>2</sub>O<sub>3</sub> content, and in changes of the pore volume and pore size, which were maximized for the CZA-La50 sample where 50% of Al<sub>2</sub>O<sub>3</sub> was replaced by La<sub>2</sub>O<sub>3</sub>. Furthermore, La-promotion resulted in an increase of the relative population and strength of basic sites of moderate strength.

The addition of La<sub>2</sub>O<sub>3</sub> generally resulted in a decrease of CO<sub>2</sub> conversion, which was less pronounced for the CZA-La50 sample, and in an increase of selectivity to methanol. The CZA-La50 catalyst exhibited the highest yields of methanol, which was 30% higher than that of the un-promoted catalyst at 210 °C. This could be attributed to the La-induced modification of the distribution of basic sites on the catalyst surface and the concomitant enhancement of the adsorption of CO<sub>2</sub> and intermediate species that were involved in the methanol formation reaction. In addition, the CZA-La50 catalyst was found to maintain a relatively large part of copper in its metallic form under reaction conditions, indicating that the presence of this phase in high relative concentrations may be related to the enhanced methanol selectivities of the La-promoted catalysts.

The results of in situ DRIFTS experiments performed in the temperature range of 25–400 °C showed that the reaction proceeded with the intermediate formation of surface formate and methoxy species. These species, which were more clearly resolved over the CZA-La50 catalyst compared to the un-promoted sample, existed on the catalyst surface at temperatures up to 200 °C, where methanol and CO formation started taking place. Based on these observations and literature results, it was proposed that the adsorbed formate was the common surface intermediate species for both methanol and CO production.

The kinetics of the reaction were studied over the best performing CZA-La50 catalyst in the temperature range of 190–230 °C under different partial pressures of CO<sub>2</sub> and H<sub>2</sub>. It was found that the increase of the partial pressure of H<sub>2</sub> at a constant partial pressure of CO<sub>2</sub> did not affect the rate of CO evolution appreciably, but resulted in an almost linear increase of the methanol formation rate. On the other hand, the increase of  $P_{\text{CO}_2}$  at constant  $P_{\text{H}_2}$  resulted in a progressive increase of the formation rates of both products. The kinetic measurements were modeled using a dual-site Langmuir–Hinshelwood mechanism according to which CO and CO<sub>2</sub> adsorbed competitively on one site (s1), whereas H<sub>2</sub> and H<sub>2</sub>O adsorbed competitively on a different site (s2). Based on the results of DRIFTS experiments, it was suggested that both methanol and CO were produced with the intermediate formation of formate species, which may either hydrogenate to yield methoxy species and, eventually, methanol, or convert to CO via the RWGS reaction. The rate expressions developed assuming that the rate-determining step (RDS) for CO production was the formation of the formate species and the RDS for methanol production was the formation of methoxy species provided the best fitting to the experimental kinetic results.

**Author Contributions:** M.K., K.K., and D.I.K. conceived of and designed the experiments; M.K. and K.K. performed the experiments; M.K., K.K., and D.I.K. analyzed the results and wrote the paper. All authors have read and agreed to the published version of the manuscript.

**Funding:** This research was performed under the research project entitled “Development of Catalysts for CO<sub>2</sub> Hydrogenation to Methanol”, which is implemented through/co-financed by the Operational Program “Human

Resources Development, Education and Lifelong Learning” and is co-financed by the European Union (European Social Fund) and Greek national funds.

**Acknowledgments:** The assistance of Theodora Ramantani, Ph.D. student at the Department of Chemical Engineering of the University of Patras, Greece, is gratefully acknowledged.

**Conflicts of Interest:** The authors declare no conflict of interest. The funders had no role in the design of the study; in the collection, analyses, or interpretation of data; in the writing of the manuscript; nor in the decision to publish the results.

## References

1. Álvarez, A.; Bansode, A.; Urakawa, A.; Bavykina, A.V.; Wezendonk, T.A.; Makkee, M.; Gascon, J.; Kapteijn, F. Challenges in the greener production of formates/formic acid, methanol, and DME by heterogeneously catalyzed CO<sub>2</sub> hydrogenation processes. *Chem. Rev.* **2017**, *117*, 9804–9838. [[CrossRef](#)]
2. Kobayashi, H.; Taylor, J.M.; Mitsuka, Y.; Ogiwara, N.; Yamamoto, T.; Toriyama, T.; Matsumura, S.; Kitagawa, H. Charge transfer dependence on CO<sub>2</sub> hydrogenation activity to methanol in Cu nanoparticles covered with metal–organic framework systems. *Chem. Sci.* **2019**, *10*, 3289–3294. [[CrossRef](#)] [[PubMed](#)]
3. Wang, W.; Wang, S.; Ma, X.; Gong, J. Recent advances in catalytic hydrogenation of carbon dioxide. *Chem. Soc. Rev.* **2011**, *40*, 3703–3727. [[CrossRef](#)] [[PubMed](#)]
4. Bowker, M. Methanol synthesis from CO<sub>2</sub> hydrogenation. *ChemCatChem* **2019**, *11*, 4238–4246. [[CrossRef](#)]
5. Tabatabaei, J.; Sakakini, B.H.; Waugh, K.C. On the mechanism of methanol synthesis and the water-gas shift reaction on ZnO. *Catal. Lett.* **2006**, *110*, 77–84. [[CrossRef](#)]
6. Behrens, M.; Studt, F.; Kasatkin, I.; Kuhl, S.; Havecker, M.; Abild-Pedersen, F.; Zander, S.; Girgsdies, F.; Kurr, P.; Knief, B.-L.; et al. The active site of methanol synthesis over Cu/ZnO/Al<sub>2</sub>O<sub>3</sub> industrial catalysts. *Science* **2012**, *336*, 893–897. [[CrossRef](#)]
7. Kattel, S.; Ramírez, P.J.; Chen, J.G.; Rodriguez, J.A.; Liu, P. Active sites for CO<sub>2</sub> hydrogenation to methanol on Cu/ZnO catalysts. *Science* **2017**, *355*, 1296–1299. [[CrossRef](#)]
8. Nakamura, J.; Uchijima, T.; Kanai, Y.; Fujitani, T. The role of ZnO in Cu/ZnO methanol synthesis catalysts. *Catal. Today* **1996**, *28*, 223–230. [[CrossRef](#)]
9. Yoshihara, J.; Parker, S.C.; Schafer, A.; Campbell, C.T. Methanol synthesis and reverse water-gas shift kinetics over clean polycrystalline copper. *Catal. Lett.* **1995**, *31*, 313–324. [[CrossRef](#)]
10. Grabow, L.C.; Mavrikakis, M. Mechanism of methanol synthesis on Cu through CO<sub>2</sub> and CO hydrogenation. *ACS Catal.* **2011**, *1*, 365–384. [[CrossRef](#)]
11. Huš, M.; Kopač, D.; Štefančič, N.S.; Jurković, D.L.; Dasireddy, V.D.B.C.; Likozar, B. Unravelling the mechanisms of CO<sub>2</sub> hydrogenation to methanol on Cu-based catalysts using first-principles multiscale modelling and experiments. *Catal. Sci. Technol.* **2017**, *7*, 5900–5913. [[CrossRef](#)]
12. Liu, L.; Yao, H.; Jiang, Z.; Fang, T. Theoretical study of methanol synthesis from CO<sub>2</sub> hydrogenation on PdCu<sub>3</sub>(111) surface. *Appl. Surf. Sci.* **2018**, *451*, 333–345. [[CrossRef](#)]
13. Kakumoto, T.; Watanabe, T. A theoretical study for methanol synthesis by CO<sub>2</sub> hydrogenation. *Catal. Today* **1997**, *36*, 39–44. [[CrossRef](#)]
14. Liu, L.; Fan, F.; Bai, M.; Xue, F.; Ma, X.; Jiang, Z.; Fang, T. Mechanistic study of methanol synthesis from CO<sub>2</sub> hydrogenation on Rh-doped Cu(111) surfaces. *Mol. Catal.* **2019**, *466*, 26–36. [[CrossRef](#)]
15. Bahruji, H.; Bowker, M.; Hutchings, G.J.; Dimitratos, N.; Wells, P.; Gibson, E.; Jones, W.; Brookes, C.; Morgan, D.; Lalev, G.M. Pd/ZnO catalysts for direct CO<sub>2</sub> hydrogenation to methanol. *J. Catal.* **2016**, *343*, 133–146. [[CrossRef](#)]
16. Li, K.; Chen, J.G. CO<sub>2</sub> hydrogenation to methanol over ZrO<sub>2</sub>-containing catalysts: Insights into ZrO<sub>2</sub> induced synergy. *ACS Catal.* **2019**, *9*, 7840–7861. [[CrossRef](#)]
17. Phongamwong, T.; Chantaprasertporn, U.; Witoon, T.; Numpilai, T.; Poo-arporn, Y.; Limphirat, W.; Donphai, W.; Dittanet, P.; Chareonpanich, M.; Limtrakul, J. CO<sub>2</sub> hydrogenation to methanol over CuO–ZnO–ZrO<sub>2</sub>–SiO<sub>2</sub> catalysts: Effects of SiO<sub>2</sub> contents. *Chem. Eng. J.* **2017**, *316*, 692–703. [[CrossRef](#)]
18. Słoczyński, J.; Grabowski, R.; Olszewski, P.; Kozłowska, A.; Stoch, J.; Lachowska, M.; Skrzypek, J. Effect of metal oxide additives on the activity and stability of Cu/ZnO/ZrO<sub>2</sub> catalysts in the synthesis of methanol from CO<sub>2</sub> and H<sub>2</sub>. *Appl. Catal. A* **2006**, *310*, 127–137. [[CrossRef](#)]

19. Hu, X.; Zhao, C.; Guan, Q.; Hu, X.; Li, W.; Chen, J. Selective hydrogenation of CO<sub>2</sub> over a Ce promoted Cu-based catalyst confined by SBA-15. *Inorg. Chem. Front.* **2019**, *6*, 1799–1812. [[CrossRef](#)]
20. Allam, D.; Bennici, S.; Limousy, L.; Hocine, S. Improved Cu- and Zn-based catalysts for CO<sub>2</sub> hydrogenation to methanol. *C. R. Chim.* **2019**, *22*, 227–237. [[CrossRef](#)]
21. Gao, P.; Li, F.; Zhao, N.; Xiao, F.; Wei, W.; Zhong, L.; Sun, Y. Influence of modifier (Mn, La, Ce, Zr and Y) on the performance of Cu/Zn/Al catalysts via hydrotalcite-like precursors for CO<sub>2</sub> hydrogenation to methanol. *Appl. Catal. A* **2013**, *468*, 442–452. [[CrossRef](#)]
22. Lam, E.; Corral-Pérez, J.J.; Larmier, K.; Noh, G.; Wolf, P.; Comas-Vives, A.; Urakawa, A.; Copéret, C. CO<sub>2</sub> hydrogenation on Cu/Al<sub>2</sub>O<sub>3</sub>: Role of the metal/support interface in driving activity and selectivity of a bifunctional catalyst. *Angew. Chem. Int. Ed.* **2019**, *58*, 13989–13996. [[CrossRef](#)]
23. Natesakhawat, S.; Lekse, J.W.; Baltrus, J.P.; Ohodnicki, P.R.; Howard, B.H.; Deng, X.; Matranga, C. Active sites and structure–activity relationships of copper-based catalysts for carbon dioxide hydrogenation to methanol. *ACS Catal.* **2012**, *2*, 1667–1676. [[CrossRef](#)]
24. Zhan, H.; Li, F.; Gao, P.; Zhao, N.; Xiao, F.; Wei, W.; Zhong, L.; Sun, Y. Methanol synthesis from CO<sub>2</sub> hydrogenation over La–M–Cu–Zn–O (M = Y, Ce, Mg, Zr) catalysts derived from perovskite-type precursors. *J. Power Sources* **2014**, *251*, 113–121. [[CrossRef](#)]
25. Hayward, J.S.; Smith, P.J.; Kondrat, S.A.; Bowker, M.; Hutchings, G.J. The effects of secondary oxides on copper-based catalysts for green methanol synthesis. *ChemCatChem* **2017**, *9*, 1655–1662. [[CrossRef](#)]
26. Guo, X.; Mao, D.; Lu, G.; Wang, S.; Wu, G. The influence of La doping on the catalytic behavior of Cu/ZrO<sub>2</sub> for methanol synthesis from CO<sub>2</sub> hydrogenation. *J. Mol. Catal. A* **2011**, *345*, 60–68. [[CrossRef](#)]
27. Yang, C.; Ren, J.; Sun, Y. Role of La<sub>2</sub>O<sub>3</sub> in Pd-supported catalysts for methanol decomposition. *Catal. Lett.* **2002**, *84*, 123–129. [[CrossRef](#)]
28. Borodko, Y.; Somorjai, G.A. Catalytic hydrogenation of carbon oxides—A 10-year perspective. *Appl. Catal. A* **1999**, *186*, 355–362. [[CrossRef](#)]
29. Toyir, J.; Miloua, R.; Elkadri, N.E.; Nawdali, M.; Toufik, H.; Miloua, F.; Saito, M. Sustainable process for the production of methanol from CO<sub>2</sub> and H<sub>2</sub> using Cu/ZnO-based multicomponent catalyst. *Phys. Procedia* **2009**, *2*, 1075–1079. [[CrossRef](#)]
30. Ma, J.; Sun, N.; Zhang, X.; Zhao, N.; Xiao, F.; Wei, W.; Sun, Y. A short review of catalysis for CO<sub>2</sub> conversion. *Catal. Today* **2009**, *148*, 221–231. [[CrossRef](#)]
31. Bonura, G.; Cordaro, M.; Cannilla, C.; Arena, F.; Frusteri, F. The changing nature of the active site of Cu–Zn–Zr catalysts for the CO<sub>2</sub> hydrogenation reaction to methanol. *Appl. Catal. B* **2014**, *152–153*, 152–161. [[CrossRef](#)]
32. An, X.; Li, J.; Zuo, Y.; Zhang, Q.; Wang, D.; Wang, J. A Cu/Zn/Al/Zr fibrous catalyst that is an improved CO<sub>2</sub> hydrogenation to methanol catalyst. *Catal. Lett.* **2007**, *118*, 264–269. [[CrossRef](#)]
33. Yoshihara, J.; Campbell, C.T. Methanol synthesis and reverse water–gas shift kinetics over Cu(110) model catalysts: Structural sensitivity. *J. Catal.* **1996**, *161*, 776–782. [[CrossRef](#)]
34. Yang, Y.; Mims, C.A.; Disselkamp, R.S.; Kwak, J.-H.; Peden, C.H.F.; Campbell, C.T. (Non)formation of methanol by direct hydrogenation of formate on copper catalysts. *J. Phys. Chem. C* **2010**, *114*, 17205–17211. [[CrossRef](#)]
35. Ramli, M.Z.; Syed-Hassan, S.S.A.; Hadi, A. Performance of Cu–Zn–Al–Zr catalyst prepared by ultrasonic spray precipitation technique in the synthesis of methanol via CO<sub>2</sub> hydrogenation. *Fuel Process. Technol.* **2018**, *169*, 191–198. [[CrossRef](#)]
36. Cai, W.; Chen, Q.; Wang, F.; Li, Z.; Yu, H.; Zhang, S.; Cui, L.; Li, C. Comparison of the promoted CuZnM<sub>x</sub>O<sub>y</sub> (M: Ga, Fe) catalysts for CO<sub>2</sub> hydrogenation to methanol. *Catal. Lett.* **2019**, *149*, 2508–2518. [[CrossRef](#)]
37. Ban, H.; Li, C.; Asami, K.; Fujimoto, K. Influence of rare-earth elements (La, Ce, Nd and Pr) on the performance of Cu/Zn/Zr catalyst for CH<sub>3</sub>OH synthesis from CO<sub>2</sub>. *Catal. Commun.* **2014**, *54*, 50–54. [[CrossRef](#)]
38. Arena, F.; Mezzatesta, G.; Zafarana, G.; Trunfio, G.; Frusteri, F.; Spadaro, L. How oxide carriers control the catalytic functionality of the Cu–ZnO system in the hydrogenation of CO<sub>2</sub> to methanol. *Catal. Today* **2013**, *210*, 39–46. [[CrossRef](#)]
39. Sun, Q.; Liu, C.-W.; Pan, W.; Zhu, Q.-M.; Deng, J.-F. In situ IR studies on the mechanism of methanol synthesis over an ultrafine Cu/ZnO/Al<sub>2</sub>O<sub>3</sub> catalyst. *Appl. Catal. A* **1998**, *171*, 301–308. [[CrossRef](#)]
40. Panagiotopoulou, P.; Kondarides, D.I.; Verykios, X.E. Mechanistic study of the selective methanation of CO over Ru/TiO<sub>2</sub> catalyst. Identification of active surface species and reaction pathways. *J. Phys. Chem. C* **2011**, *115*, 1220–1230. [[CrossRef](#)]

41. Le Peltier, F.; Chaumette, P.; Saussey, J.; Bettahar, M.M.; Lavalley, J.C. In situ FT-IR and kinetic study of methanol synthesis from CO/H<sub>2</sub> over ZnAl<sub>2</sub>O<sub>4</sub> and Cu–ZnAl<sub>2</sub>O<sub>4</sub> catalysts. *J. Mol. Catal. A* **1998**, *132*, 91–100. [[CrossRef](#)]
42. Sanchez-Escribano, V.; Larrubia Vargas, M.A.; Finocchio, E.; Busca, G. On the mechanisms and the selectivity determining steps in syngas conversion over supported metal catalysts: An IR study. *Appl. Catal. A* **2007**, *316*, 68–74. [[CrossRef](#)]
43. Schumann, J.; Eichelbaum, M.; Lunkenbein, T.; Thomas, N.; Alvarez Galvan, M.C.; Schlogl, R.; Behrens, M. Promoting strong metal support interaction: Doping ZnO for enhanced activity of Cu/ZnO:M (M=Al, Ga, Mg) catalysts. *ACS Catal.* **2015**, *5*, 3260–3270. [[CrossRef](#)]
44. Fang, X.; Men, Y.; Wu, F.; Zhao, Q.; Singh, R.; Xiao, P.; Du, T.; Webley, P.A. Moderate-pressure conversion of H<sub>2</sub> and CO<sub>2</sub> to methanol via adsorption enhanced hydrogenation. *Int. J. Hydrogen Energy* **2019**, *44*, 21913–21925. [[CrossRef](#)]
45. Xiao, J.; Mao, D.; Guo, X.; Yu, J. Effect of TiO<sub>2</sub>, ZrO<sub>2</sub>, and TiO<sub>2</sub>–ZrO<sub>2</sub> on the performance of CuO–ZnO catalyst for CO<sub>2</sub> hydrogenation to methanol. *Appl. Surf. Sci.* **2015**, *338*, 146–153. [[CrossRef](#)]
46. Li, C.; Yuan, X.; Fujimoto, K. Development of highly stable catalyst for methanol synthesis from carbon dioxide. *Appl. Catal. A* **2014**, *469*, 306–311. [[CrossRef](#)]
47. Din, I.U.; Shaharun, M.S.; Alotaibi, M.A.; Alharthi, A.I.; Naeem, A. Recent developments on heterogeneous catalytic CO<sub>2</sub> reduction to methanol. *J. CO<sub>2</sub> Util.* **2019**, *34*, 20–33. [[CrossRef](#)]
48. Saito, M.; Fujitani, T.; Takeuchi, M.; Watanabe, T. Development of copper/zinc oxide-based multicomponent catalysts for methanol synthesis from carbon dioxide and hydrogen. *Appl. Catal. A* **1996**, *138*, 311–318. [[CrossRef](#)]
49. Liu, Y.-M.; Liu, J.-T.; Liu, S.-Z.; Li, J.; Gao, Z.-H.; Zuo, Z.-J.; Huang, W. Reaction mechanisms of methanol synthesis from CO/CO<sub>2</sub> hydrogenation on Cu<sub>2</sub>O(111): Comparison with Cu(111). *J. CO<sub>2</sub> Util.* **2017**, *20*, 59–65. [[CrossRef](#)]
50. Dasireddy, V.B.C.D.; Likozar, B. The role of copper oxidation state in Cu/ZnO/Al<sub>2</sub>O<sub>3</sub> catalysts in CO<sub>2</sub> hydrogenation and methanol productivity. *Renew. Energy* **2019**, *140*, 452–460. [[CrossRef](#)]
51. Fisher, I.A.; Woo, H.C.; Bell, A.T. Effects of zirconia promotion on the activity of Cu/SiO<sub>2</sub> for methanol synthesis from CO/H<sub>2</sub> and CO<sub>2</sub>/H<sub>2</sub>. *Catal. Lett.* **1997**, *44*, 11–17. [[CrossRef](#)]
52. Hong, Q.J.; Liu, Z.P. Mechanism of CO<sub>2</sub> hydrogenation over Cu/ZrO<sub>2</sub>(212) interface from first-principles kinetics Monte Carlo simulations. *Surf. Sci.* **2010**, *604*, 1869–1876.
53. Graaf, G.H.; Stamhuis, E.J.; Beenackers, A.A.C.M. Kinetics of low-pressure methanol synthesis. *Chem. Eng. Sci.* **1988**, *43*, 3185–3195. [[CrossRef](#)]
54. Graaf, G.H.; Scholtens, H.; Stamhuis, E.J.; Beenackers, A.A.C.M. Intra-particle diffusion limitations in low-pressure methanol synthesis. *Chem. Eng. Sci.* **1988**, *45*, 773–783. [[CrossRef](#)]
55. Tisseraud, C.; Comminges, C.; Belin, T.; Ahouari, H.; Soualah, A.; Pouilloux, Y.; Le Valant, A. The Cu–ZnO synergy in methanol synthesis from CO<sub>2</sub>, Part 2: Origin of the methanol and CO selectivities explained by experimental studies and a sphere contact quantification model in randomly packed binary mixtures on Cu–ZnO coprecipitate catalysts. *J. Catal.* **2015**, *330*, 533–544. [[CrossRef](#)]
56. Dasireddy, V.D.B.C.; Štefančič, N.S.; Huš, M.; Likozar, B. Effect of alkaline earth metal oxide (MO) Cu/MO/Al<sub>2</sub>O<sub>3</sub> catalysts on methanol synthesis activity and selectivity via CO<sub>2</sub> reduction. *Fuel* **2018**, *233*, 103–112. [[CrossRef](#)]
57. Liu, C.; Guo, X.; Guo, Q.; Mao, D.; Yu, J.; Lu, G. Methanol synthesis from CO<sub>2</sub> hydrogenation over copper catalysts supported on MgO-modified TiO<sub>2</sub>. *J. Mol. Catal. A* **2016**, *425*, 86–93. [[CrossRef](#)]
58. Graaf, G.H.; Sijtsema, P.J.J.M.; Stamhuis, E.J.; Joosten, G.E.H. Chemical equilibria in methanol synthesis. *Chem. Eng. Sci.* **1986**, *41*, 2883–2890. [[CrossRef](#)]
59. Boudart, M.; Djega-Mariadassou, G. *Kinetics of Heterogeneous Catalytic Reactions*; Princeton University Press: Princeton, NJ, USA, 1984.
60. Karelavic, A.; Ruiz, P. The role of copper particle size in low pressure methanol synthesis via CO<sub>2</sub> hydrogenation over Cu/ZnO catalysts. *Catal. Sci. Technol.* **2015**, *5*, 869–881. [[CrossRef](#)]

